PCCP

The Role of the Dipolar Neighborhood on the Relaxation Dynamics of Multichromophoric Merocyanines

Journal:	*Physical Chemistry Chemical Physics*
Manuscript ID	CP-ART-04-2016-002437.R2
Article Type:	Paper
Date Submitted by the Author:	23-Jun-2016

Complete List of Authors:	Koch, Federico; Universität Würzburg, Institut für Physikalische und Theoretische Chemie Steinbacher, Andreas; Universität Würzburg, Institut für Physikalische und Theoretische Chemie Consani, Cristina; Universität Würzburg, Institut für Physikalische Chemie; CTR - Carinthian Tech Research AG Zitzler-Kunkel, André; Universität Würzburg, Institute of Organic Chemistry Stolte, Matthias; Universität Würzburg, Institute of Organic Chemistry Würthner, Frank; Universität Würzburg, Institute of Organic Chemistry Brixner, Tobias; Universität Würzburg, Institut für Physikalische Chemie

Journal Name

ARTICLE TYPE

Cite this: DOI: 10.1039/xxxxxxxxxx

The Role of the Dipolar Neighborhood on the Relaxation Dynamics of Multichromophoric Merocyanines

Federico Koch,[a] Andreas Steinbacher,[a] Cristina Consani,[‡ab] André Zitzler-Kunkel,[c] Matthias Stolte,[bc] Frank Würthner,[*bc] and Tobias Brixner[*ab]

Received Date
Accepted Date

DOI: 10.1039/xxxxxxxxxx

www.rsc.org/journalname

The interactions between different chromophores within a molecular system are crucial to comprehend relaxation dynamics, regardless if one deals with small molecules or larger systems like polymers or aggregates. We investigate a series of merocyanine molecules that contain one, two or three highly dipolar ($\mu_g = 13.1$ D) dyes in close vicinity to study the influence and origin of interactions, e.g., electronic, vibronic, or the formation of excitons. Relaxation dynamics are probed via transient absorption and coherent two-dimensional spectroscopy. Furthermore, we derive a general relaxation model which can be applied for all merocyanines under investigation and can be used as a reference point for other dipolar donor–acceptor dyes. The intramolecular charge-transfer state of the monomeric merocyanine is stabilized by dipolar neighbor molecules in the bis- and tris-chromophoric dyes.

1 Introduction

Chromophores which are in proximity to each other are known to interact in various ways. Attractive interactions can lead to the formation of aggregates that display distinct changes in their linear absorption spectra compared to their monomeric units. Such a behavior can be described by the formation of excitons.[1] Furthermore, a chromophore can act as an energy donor and transfer excitation energy to another energy acceptor chromophore. The theoretical description of energy transfer can be complicated in general, but often used limiting cases are Förster[2] and Dexter[3] energy transfer. In addition to energy, electrons can be transferred from one chromophore to another. For chemically linked chromophores electron transfer results in charge-transfer (CT) states. Such CT states are not limited to electron transfer between two different chromophores, but can also occur within one chromophore in so-called push–pull chromophores as given for merocyanine dyes, which create an intramolecular charge-transfer (ICT) state.[4] All these interactions lead to particular signatures in spectroscopic measurements. However, it is often rather complicated to ascertain the true origin of the observed spectroscopic changes. Hence, this study aims at a systematic investigation of the chromophore–chromophore interaction by synthesizing a series of multichromophoric merocyanine dyes that are then compared.

Merocyanines consist of a polymethine bridge, variable in length, with an attached terminal electron donor (D) and electron acceptor (A) moiety at each end. These donor–acceptor (D–A) systems consist of an even number of π electrons and an odd number of π-center groups.[5] Versatile options of structural variation enable fine tuning of electronic and optical properties. Therefore, a large field of applications is accessible, e.g., in biology and medicine,[6] nonlinear optics and photorefractive materials,[7,8] and as organic p-semiconducting materials in organic solar cells and field-effect transistors.[9–12] Due to the delocalization of π electrons in merocyanines over D, A, and the polymethine bridge, it is possible to describe the π system with two molecular resonance structures: firstly, a neutral polyene and secondly, a zwitterionic (or betaine) structure.[6] The contribution of the two resonance structures can be influenced by varying the chemical structure(s) of the D and A moiety(-ies) and by changing the length of the connecting polymethine linker, and to some extent by the solvent.[13] Weak electron donating (withdrawing) D (A) functional groups lead to polyene-type dyes that can vary in their molecular size. Similarly, the elongation of the connecting polymethine chain favors the neutral resonance structure, due to an exacerbated charge separation between D and A. On the other hand, the exchange of the D (A) moiety with a stronger electron donating (withdrawing) group leads to merocyanines with equal contribu-

[a] *Institut für Physikalische und Theoretische Chemie, Universität Würzburg, Am Hubland, 97074 Würzburg, Germany. Fax: +49 931 31-86332; Tel: +49 931 31-86330; E-mail: brixner@phys-chemie.uni-wuerzburg.de*

[b] *Center for Nanosystems Chemistry (CNC), Universität Würzburg, Am Hubland, 97074 Würzburg, Germany*

[c] *Institut für Organische Chemie, Universität Würzburg, Am Hubland, 97074 Würzburg, Germany. Fax: +49 931 31-84756; Tel: +49 931 31-85340; E-mail: wuerthner@chemie.uni-wuerzburg.de*

[‡] *Present address: CTR - Carinthian Tech Research AG, Europastraße 12, 9524 Villach, Austria*

[*] *Author to whom the correspondence should be addressed*

tions of the neutral and the zwitterionic resonance structures. The latter scenario is called "cyanine limit". Merocyanines in the cyanine limit display the smallest reorganization energies [14] and the highest transition dipole moments [7] in comparison to the other resonance structures, which leads to sharp absorption bands and almost no geometrical changes upon electronic excitation.

Merocyanine and cyanine dyes often exhibit rather complex relaxation dynamics in solution. Recent studies of merocyanine and cyanine derivatives revealed isomerization processes due to a rotation along a double bond of the polymethine bridge [15–20], as well as ultrafast ring-closure and -opening events from a merocyanine to a spiro compound (ring-closed form). [21–24] Furthermore, it is known that conical intersections can accelerate the relaxation pathways, [25–29] and also the influence of protonation of merocyanines on the relaxation dynamics was studied. [30] Moreover, the ultrafast deactivation to a hot ground state, strongly depending on the environment (solvent), was investigated. [31]

The present work goes beyond those monochromophoric studies and deals with chromophore–chromophore interactions between merocyanine dyes. Typically, these interactions can lead to shifts of the absorption bands and to changes of their relative intensities. Thus, a systematic merocyanine series (Fig. 1a) was investigated, beginning with a single merocyanine chromophore consisting of an indolenine D (red) and a thiazol A moiety (blue).‡ The A is directly linked to a benzene unit, which allows connecting further chemically identical merocyanine chromophores. The monomer (**1**) acts as a reference dye (since in this case chromophore–chromophore interactions are absent) for the multichromophore dyes (**2p**, **2m**, and **3**). Chromophore–chromophore interactions are introduced for bis-merocyanines, which are connected in para (**2p**) and meta (**2m**) position to each other, and a tris-merocyanine (**3**) for which all chromophores are in meta position to each other.

Figure 1b shows the linear absorption spectra in dichloromethane (DCM) of the investigated merocyanine dyes. In the following, we focus on spectral changes in the range from $\approx 500-750$ nm. The linear absorption spectrum of the monomer **1** (red in Fig. 1b) displays an absorption maximum at $\lambda_{max} = 633$ nm. Furthermore, additional absorption bands around 595 nm and 540 nm can be attributed to a vibrational progression of the $S_0 \rightarrow S_1$ transition. In comparison to **1**, the para-linked dye **2p** (blue in Fig. 1b) displays a 12 nm bathochromically shifted absorption maximum at $\lambda_{max} = 645$ nm with a small additional absorption band at 602 nm. The bathochromic shift of λ_{max} for a two-chromophore system in comparison to a monomer indicates either a J-type excitonic coupling of the two chromophores [1] or an increased conjugation length of the π-electron system. In contrast to **2p**, the meta-linked dye, **2m** (brown in Fig. 1b), displays a hypsochromically shifted absorption maximum at $\lambda_{max} = 626$ nm with an intense additional absorption band at 593 nm. Lastly, the trimer **3** (green in Fig. 1b), for which all three chromophores are in meta position to each other, displays the most complex absorption spectrum. On the blue edge, the absorption maximum

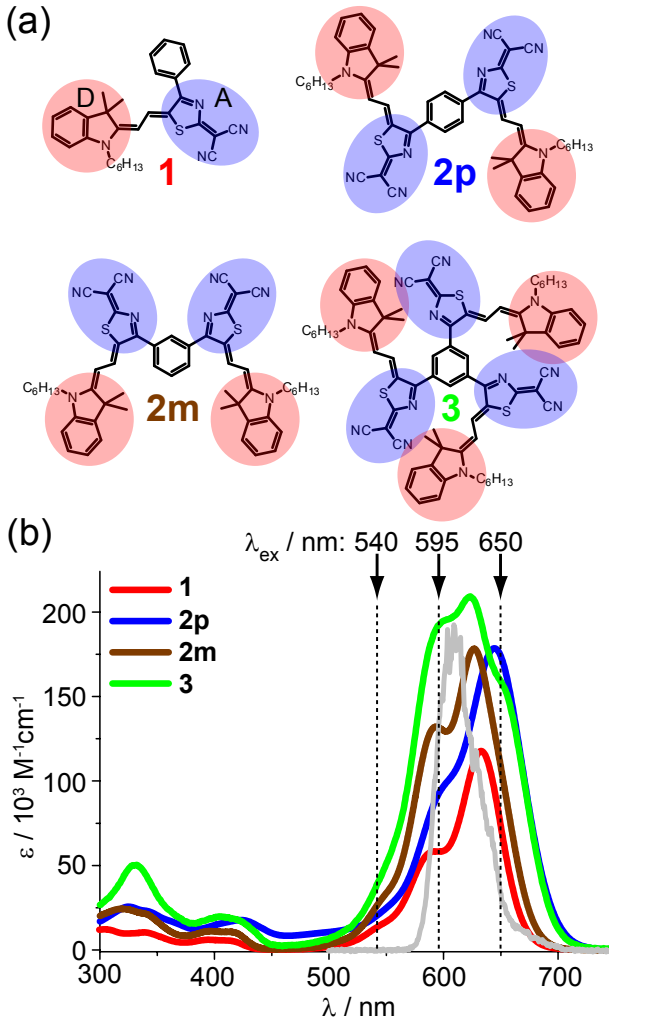

Fig. 1 (a) Chemical structures of the studied monomer (**1**), consisting of an indolenine D (red) and a thiazol A moiety (blue), and multichromophore (**2p**, **2m**, and **3**) dyes. Labels next to the chemical structures describe the number of chromophores. To distinguish the bis-merocyanines (**2**), the binding site relative to the other chromophore is labeled additionally (m = meta, p = para). The chromophores of **3** are all linked to each other in meta position at the benzene unit. (b) Linear absorption spectra for all dyes dissolved in DCM, displaying strong differences in their absorption maxima (λ_{max}) and relative absorption band intensities. The experiments of Sections 2.1, 2.2, and 2.4 were performed with the laser spectrum depicted in gray. Black arrows and dashed lines indicate the different laser excitation wavelengths (λ_{ex}) of spectrally narrow pulses, which were set to determine the effect of excess energy on the molecular relaxation dynamics (Sec. 2.3).

at $\lambda_{max} = 623$ nm with an additional absorption band at 598 nm is similar to the absorption features of **2m**, on the red edge the third bathochromically shifted band at ≈ 652 nm is more similar to λ_{max} of **2p**.

To be able to comprehend these changes in the linear absorption spectra and thus the origin of the chromophore–chromophore interactions, we investigate the ultrafast dynamics (see Sec. 5 on Materials and Methods) depending on the substitution pattern. The relaxation dynamics of the single merocyanine **1** in solution are investigated by transient absorption (TA) spectroscopy (Sec. 2.1) and subsequently compared to both bis-

‡ The synthesis will be described in a forthcoming paper. [32]

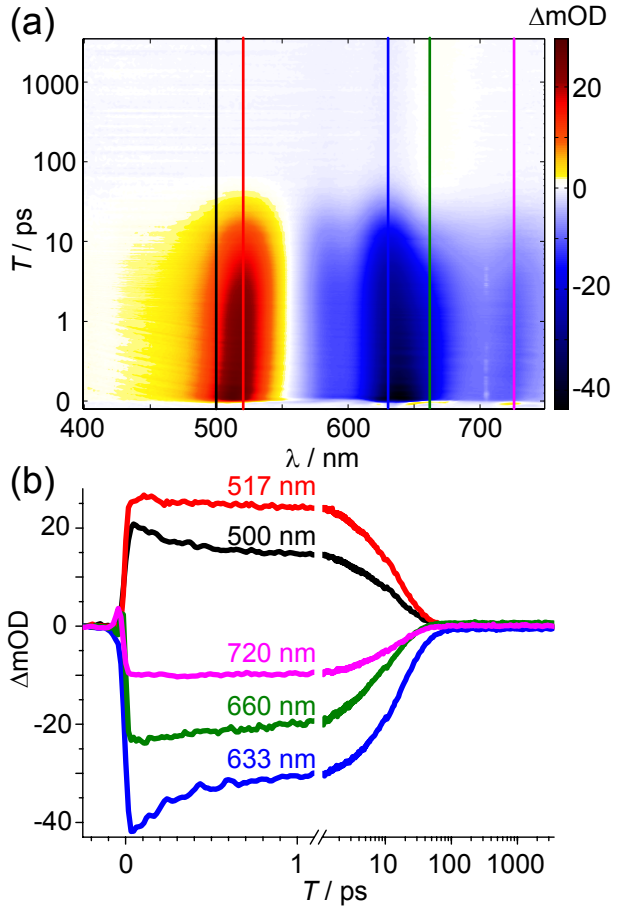

Fig. 2 (a) Chirp-corrected transient absorption (TA) map of the monomer **1** in DCM upon 630 nm excitation as a function of detection wavelength λ and waiting time T. The T axis is plotted in linear scale up to 1 ps and logarithmically afterwards. Negative signals (blue/black) in the region of $550-750$ nm correspond to ground-state bleach (GSB) and stimulated emission (SE), positive signals (yellow/red) around $400-550$ nm originate from excited-state absorption (ESA). The "uneven" vertical signal at ≈ 705 nm is due to a defective pixel of the CCD camera in the spectrometer. (b) Exemplary transients [included as colored vertical lines in (a)] display the time evolution of the signals at certain wavelengths. Transients are plotted linearly up to 1.1 ps and logarithmically afterwards, which is indicated by a double break in the T axis, without neglecting data points.

and the tris-merocyanine (Sec. 2.2). The influence of the excitation energy on the relaxation is investigated in Sec. 2.3 for all merocyanines. Furthermore, the results of coherent 2D spectroscopy (Sec. 2.4) in TA geometry are presented. All experimental results are interpreted and discussed afterwards in Sec. 3. Finally, we summarize the key observations in Sec. 4.

2 Experimental Data

2.1 Relaxation Dynamics of the Mono-Merocyanine 1

Figure 2a depicts the TA map of **1** upon excitation with pulses centered at 630 nm (see gray spectrum in Fig. 1b). Negative signals (blue/black) in the region of $550-750$ nm correspond to ground-state bleach (GSB) and stimulated emission (SE), positive signals (yellow/red) around $400-550$ nm originate from excited-state absorption (ESA). Initially, an ultrafast (≈ 200 fs) relaxation is observable as the ESA and SE shift towards longer wavelengths. Subsequently, the signal decays within tens of picoseconds, resulting in a small remaining signal (≈ 0.75 mOD) of GSB at 633 nm and photoinduced absorption at 660 nm up to a maximum delay of 3.6 ns. Corresponding kinetic traces at selected wavelengths are presented in Fig. 2b. The initial ultrafast relaxation is observable through a different signal evolution in the ESA for 500 nm (black) and 517 nm (red). The shift of the SE is visible as a small initial rise at 660 nm (green) and 720 nm (pink). Furthermore, oscillatory behavior can be observed at 633 nm (blue, GSB) during the first 2 ps.[33] To achieve a more detailed interpretation of the relaxation dynamics of **1**, we performed a global analysis of the time-resolved data. Five decay times were prerequisite to fit the data properly. In order to account for permanent remaining signal contributions, one of the time scales was fixed at 10 ns, which is larger than our experimentally accessible delay time. The additional time constants for **1** were found to be $\tau_1 = 213$ fs, $\tau_2 = 1.4$ ps, $\tau_3 = 10$ ps, and $\tau_4 = 17$ ps.

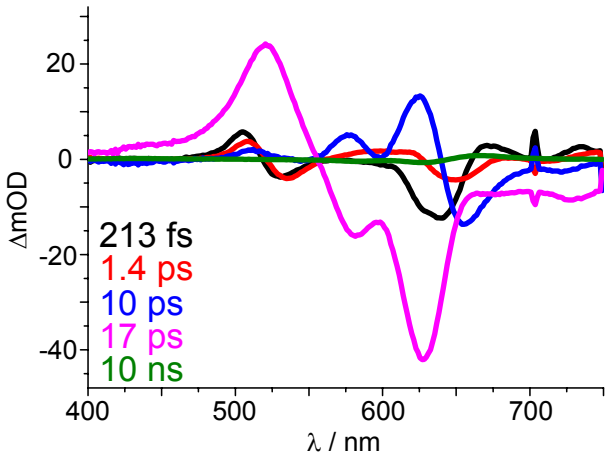

Fig. 3 DADS and corresponding relaxation times of **1** in DCM upon 630 nm excitation. Five time components are necessary to describe the data properly. The 10 ns time component (green) was fixed to describe the remaining signal at a maximal population time of $T = 3.6$ ns. The "uneven" signal at ≈ 705 nm is due to a defective pixel of the CCD camera in the spectrometer.

Figure 3 shows the decay-associated difference spectra (DADS) for **1** upon 630 nm excitation. The DADS of the ultrafast (213 fs) decay (black) possesses negative contributions around 535 and 635 nm and positive ones around 505, 675 and 735 nm. The shape of the DADS for such an ultrashort time constant leads to the conclusion that the system performs an initial motion away from the Franck–Condon region towards lower-energetic regions of the S_1 potential energy surface (PES). The $\tau_2 = 1.4$ ps component (red) displays a shift towards larger wavelengths in the ESA ($510-535$ nm) and SE ($650-745$ nm) regions. This process can be assigned to vibrational cooling. The $\tau_3 = 10$ ps component (blue) displays a small rise of ESA at 435 nm and a loss of ESA at 515 nm. Furthermore, the SE decays at 658 and 725 nm. The spectral shape of the 10 ps DADS indicates a shift of the GSB and SE signals to shorter wavelengths as the SE decreases stronger than the GSB. The $\tau_4 = 17$ ps component (pink) has

the largest amplitude of all DADS. Displaying ESA (< 550 nm), GSB ($550-660$ nm), and SE (> 660 nm) features, it describes the decay of excited-state population to the ground state as all contributions decrease almost completely. The ESA feature can be attributed to the absorption from the first excited state (S_1) to energetically higher-lying excited states (S_n). Furthermore, the 17 ps component displays a shallow and unstructured SE from $660-750$ nm. As mentioned above, the $\tau_5 = 10$ ns component (green) describes a small remaining signal (< 1 mOD) which consists of a GSB and a photo-induced absorption component at 670 nm.

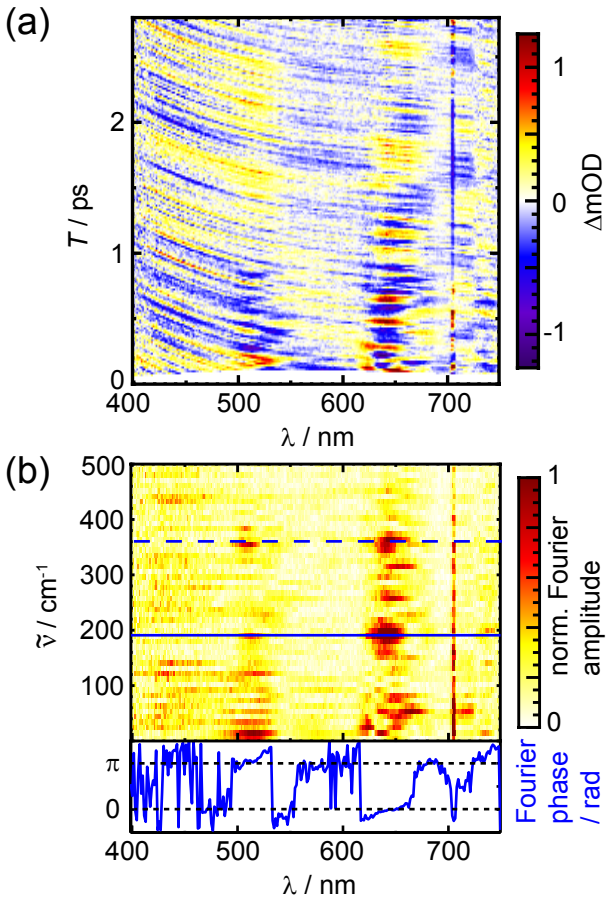

Fig. 4 (a) Fit residuals of the chirp-corrected TA map of Fig. 2a as a function of probe wavelength λ and delay time T up to 2.8 ps. Data up to $T = 50$ fs were neglected to exclude distortions of the coherent artifact. Alternating positive (yellow) and negative (blue) signals along T at $\approx 500-550$ nm and $\approx 620-750$ nm indicate signatures of a coherent vibrational wave packet. (b) Absolute values of the Fourier transform (top) of the residuals along T, displaying distinct amplitudes at 190 cm^{-1} (horizontal solid line) and 360 cm^{-1} (horizontal dashed line), respectively. The phase at 190 cm^{-1} is depicted as a function of probe wavelength λ (bottom). The "uneven" vertical signal at ≈ 705 nm is due to a defective pixel of the CCD camera in the spectrometer.

The transient at 633 nm in Fig. 2b displays distinct oscillations with a period of ≈ 200 fs which decay within the first 2 ps.[33] Such behavior was interpreted as wave-packet motion on the excited-state PES in other merocyanine dyes.[18,19] Hence, in order to analyze the observed wave-packet dynamics, the underlying decay contribution (determined by the global fit of Fig. 3) was subtracted from the raw data. The remaining fit residuals as a function of probe wavelength λ and pump–probe delay T, up to 2.8 ps, are shown in Fig. 4a. Distinct oscillations along T are visible in the ESA region at $\approx 500-550$ nm and in the GSB and SE region at $\approx 620-750$ nm as alternating positive (yellow/red) and negative signals (blue) along T. Prior to a Fourier transformation along T, TA data up to $T = 50$ fs were neglected to exclude distortions in the fit residuals due to the coherent artifact at $T = 0$. Figure 4b shows the Fourier transform of the fit residuals along T, yielding two major modes at $\tilde{\nu} = 190$ and 360 cm^{-1}. In the already mentioned recent study of similar dyes, these two modes were assigned to a torsional and vibrational stretching motion, respectively.[18,19] The resulting phase at the horizontal cut at $\tilde{\nu} = 190$ cm^{-1} of the Fourier-transformed data is shown in the bottom of Fig. 4b. Two phase jumps of $\Delta\Phi \approx \pi$ are observable at 533 and 666 nm.[33] These phase jumps correspond to the minimum of the amplitude between the turning points of an oscillating wave packet as observed in another merocyanine system[18,19] and also in other molecular systems.[34,35] The maxima of the amplitudes can be assigned to the spectral signatures at the turning points of the wave packet. At one of the turning points an increased transient population with SE at 642 nm and ESA at 512 nm can be observed, whereas on the other reversal point the SE at 682 nm and ESA at 543 nm are enhanced. Thus, we assign the oscillating features to a wave-packet motion in the excited state, as the signatures appear in the spectral regions of ESA and SE.

2.2 Relaxation Dynamics of 2p, 2m, and 3

Transient absorption maps and DADS for **2p**, **2m**, and **3** are shown in Fig. 5 (left). Similar to the TA map of **1** (Fig. 2a), all dyes display a (spectrally) broad ESA ($\approx 400-565$ nm) and combined GSB and SE ($\approx 565-720$ nm) signals. Furthermore, a shift towards shorter wavelengths is observable from $\approx 10-100$ ps for the GSB and SE band.

Like for the monomer (**1**) five decay time constants were needed to fit the relaxation dynamics properly for all other molecules (**2p**, **2m**, and **3**). The results of the global analysis are depicted as DADS (like in Fig. 3) in Fig. 5 (right) for the multichromophore dyes. All dyes display similar relaxation dynamics and spectral changes. The ultrafast relaxation processes occur with ≈ 175 fs and ≈ 1 ps. Subsequently, all dyes are still in the excited state, deducible from the distinct SE and ESA with a lifetime of $10-17$ ps. From the latter excited state two different processes are observable: a partial recovery of the ground state and the appearance of a new ESA at $\approx 400-500$ nm, accompanied by a SE with unstructured, shallow spectral shape. Despite the similar spectral behavior, the lifetime of the excited state is significantly different for the different molecules as it rises from 17 ps (**1**) over 51 ps (**2p**) up to 77 ps (**2m**) and 81 ps (**3**). Furthermore, a 10 ns component (fixed during global analysis) was needed to describe the small (< 1 mOD) remaining GSB and photoinduced absorption signal for all dyes.

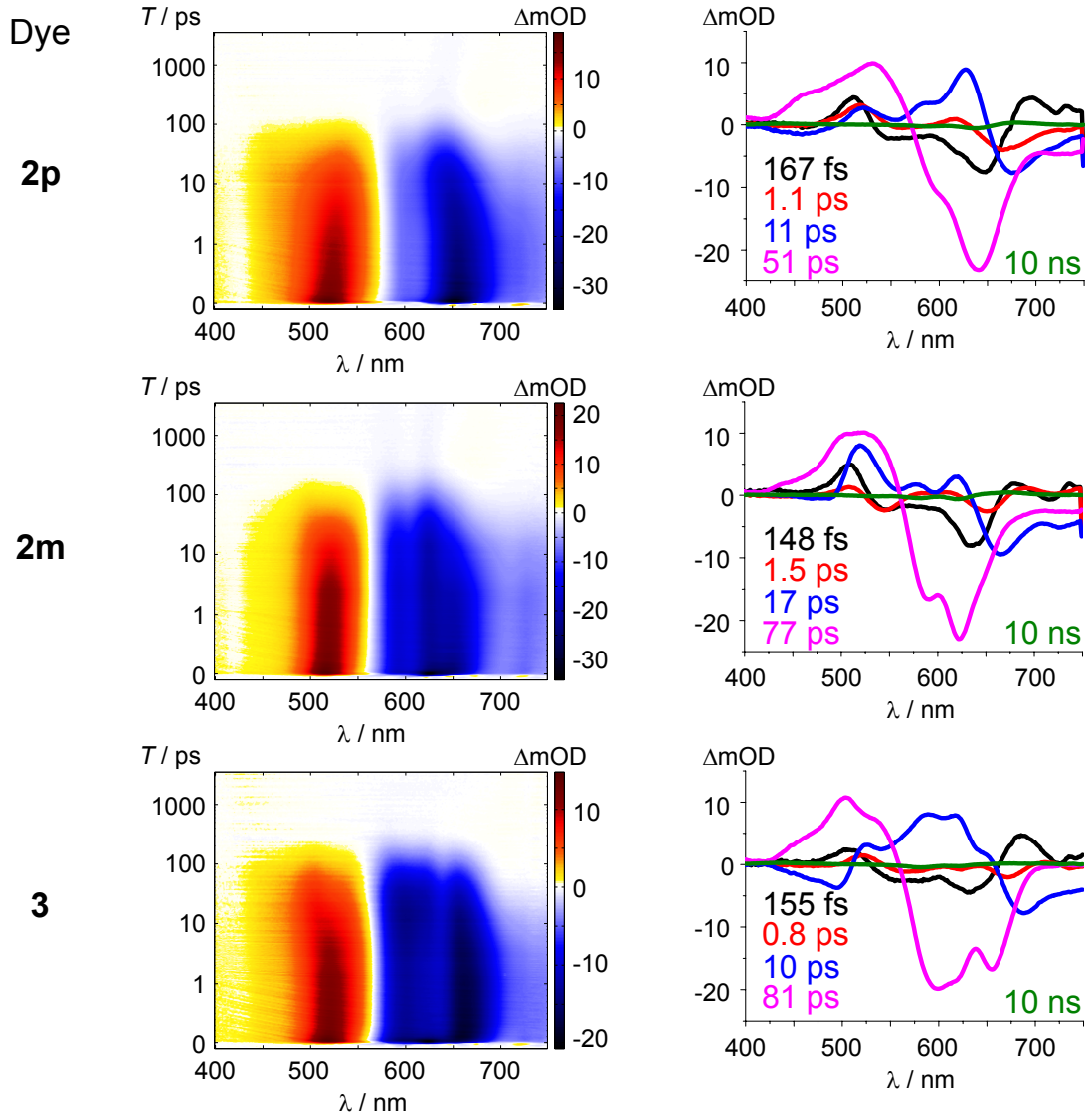

Fig. 5 Left side: TA maps of **2p**, **2m**, and **3** (from top to bottom) in DCM upon 630 nm excitation. Negative signals (blue/black) in the region of $550-750$ nm correspond to GSB and SE, positive signals (yellow/red) around $400-550$ nm originate from ESA. The T axis is plotted with a linear scale up to 1 ps and logarithmically afterwards. Right side: DADS and relaxation time scales resulting from global analysis. Five time components are necessary to describe the data properly. The 10 ns time component (green) was fixed to describe the tiny remaining signal at $T = 3.6$ ns. The "uneven" signal at ≈ 750 nm is due to a defective pixel of the CCD camera in the spectrometer.

2.3 Influence of Excitation Wavelength

In order to investigate the influence of excess energy on the relaxation dynamics, we performed TA measurements with narrowband ($\approx 15-30$ nm) fs laser pulses centered at 540 nm, 595 nm, and 650 nm, as depicted by arrows in Fig. 1b. Similar to the 633 nm excitation in the previous Sections 2.1 and 2.2, five decay times were necessary to model the time-resolved data properly. The DADS and relaxation time scales estimated from a global fit are depicted in Fig. 6. The general results and interpretation are comparable to the previous detailed discussion. Hence, here we focus on the qualitative trends of the relaxation time scales upon different excitation wavelength.

Comparing the results for the individual dyes in Fig. 6 to the previously observed relaxation dynamics (cf. Fig. 3 and Fig. 5), the three longest time components τ_3, τ_4, and τ_5 (blue, pink, and green DADS in Fig. 6, respectively) display similar spectral and temporal behavior independently of the excitation wavelength. The fixed 10 ns component (τ_5, green) is necessary to fit the remaining GSB and photoinduced absorption and does not change with varying excitation energy. Furthermore, τ_4 (pink) reflects the lifetime in the excited state, while the EADS and DADS of τ_3 (blue) show the loss of SE and a decrease of GSB. Comparing the relaxation time scales and spectral behavior, the three latter relaxation processes (τ_3, τ_4, τ_5) only display minor dependence on the excitation wavelength.

In clear contrast, the first and second relaxation times τ_1 and τ_2 (black and red DADS in Fig. 6, respectively) show a significant dependence on the excitation wavelength. For all dyes a smaller excitation wavelength (higher excitation energy) leads to a decrease of the relaxation time scale for both initial relaxation times.

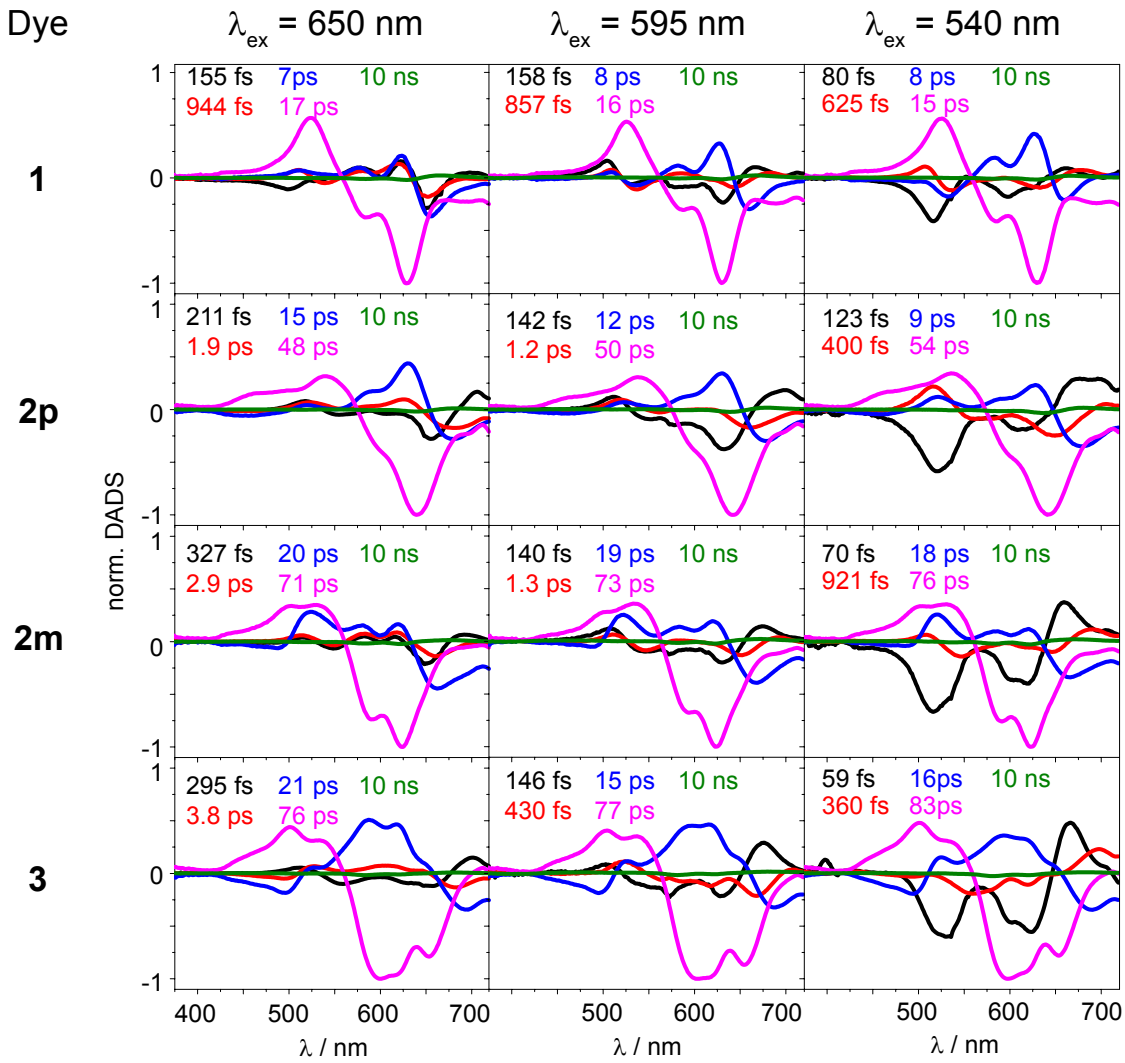

Fig. 6 Overview of DADS and relaxation times (included in the plots) resulting from global analysis for all dyes (different rows, in the order **1**, **2p**, **2m**, **3** from top to bottom) at different excitation wavelengths λ_{ex} (different columns), namely 650 nm (left), 595 nm (middle), and 540 nm (right). The longest time scale, 10 ns, was kept fixed during fitting to resemble the tiny offset signal for large T values.

The first relaxation time scale τ_1 decreases from a few hundred fs down to a sub-100 fs component. Similarly, the subsequent relaxation τ_2 decreases from a few ps at 650 nm excitation down to a sub-ps time scale at 540 nm. Hence, excitation with higher energy leads to faster initial relaxation. It is difficult to discriminate one concrete process, which leads to this wavelength dependency, as it can either imply a relaxation via an energetic barrier which has to be overcome,[30] a different initial starting point on the PES, or it can comprise ultrafast dynamics due to an intramolecular charge-transfer (ICT) state known to be formed by merocyanines.

2.4 2D Spectroscopy

Coherent 2D spectroscopy gives access to additional information in comparison to TA spectroscopy, as not only the detection axis for every waiting/population time T is energy-resolved, but also the excitation axis. Thus, this auxiliary observable of the correlation between excitation and detection energy allows direct identification of couplings between different absorption bands and the influence of the excitation energy on dynamics. More specifically, one can deduce the energy transfer between different states and observe chemical processes, e.g., a photoinduced isomerization of an initially excited reactant as observed for in previous studies of our own on similar merocyanine dyes.[18–20]

Figure 7 shows 2D spectra for all dyes of this study at selected T, ranging from 30 fs (left column) up to 70 ps (right column). To facilitate the comparison to the previous TA studies, signals corresponding to GSB and SE (blue/black) are plotted as negative signals, while ESA contributions (yellow/red) are plotted as positive signals.

At $T = 30$ fs all dyes display strong diagonal ($|\tilde{\nu}_\tau| = |\tilde{\nu}_t|$, compare black line) signal contributions, which are coupled to distinct SE features at $\tilde{\nu}_t \approx 1.4 \times 10^4$ cm^{-1} and ESA features at $\tilde{\nu}_t \approx 1.9 \times 10^4$ cm^{-1}, respectively, rather independently of $\tilde{\nu}_\tau$. With evolving population time T, the 2D signal for all dyes changes from a diagonally elongated 2D signal at $T = 30$ fs to horizontally orientated peaks at $T \approx 1$ ps. From $T = 1$ ps up to $T = 70$ ps, besides an overall signal decay, a vertical shift to

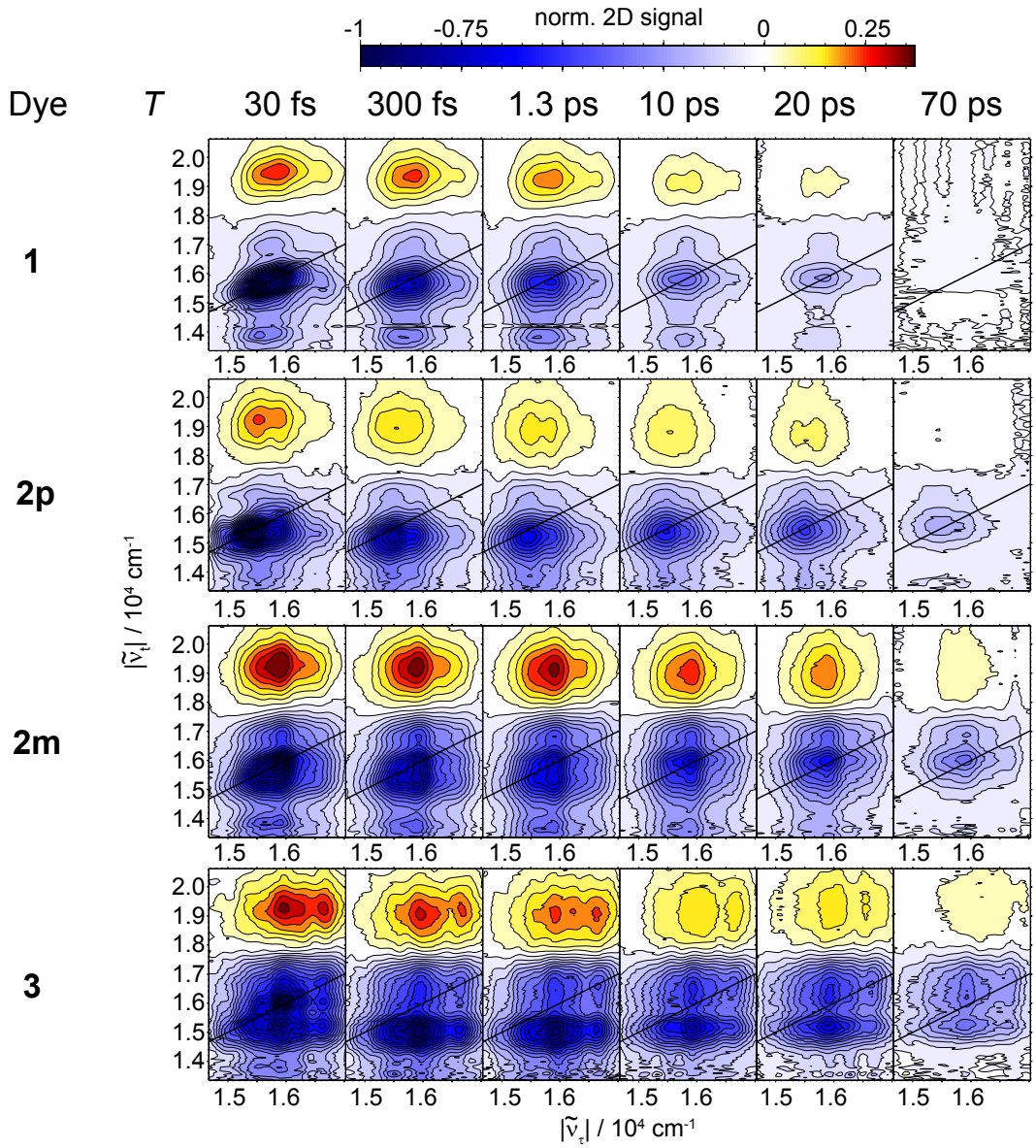

Fig. 7 Absorptive 2D spectra for (from top to bottom row) **1**, **2p**, **2m**, and **3**, are plotted as a function of excitation $\tilde{\nu}_\tau$ and detection wavenumber $\tilde{\nu}_t$ for selected population times (different columns). Negative signals (blue/black) are plotted to correspond to ground-state bleach (GSB) and stimulated emission (SE), positive signals (yellow/red) originate from excited-state absorption (ESA). Contours are plotted in steps of 5% of the maximal, normalized signal at $T = 30$ fs.

higher $\tilde{\nu}_t$ of the GSB and SE signal can be observed. Similar to the observations and interpretations of the previous TA studies, this shift can be explained by a faster decay of SE, at lower $\tilde{\nu}_t$ than the remaining GSB, during the relaxation processes. After $T \approx 1$ ps all dyes display only a minor wavelength dependence of the 2D signal. This is in distinct difference to previously studied merocyanine systems, which displayed excitation-wavenumber-dependent signatures for a photoinduced isomerization.[18,19] Thus, coherent 2D spectroscopy allows the exclusion of an isomer equilibrium in solution prior to excitation and photoinduced isomerization reactions as dominant reaction channels for all investigated dyes of this study.

Regarding the interaction between the different absorption bands (compare Fig. 1) the 2D signals for the corresponding range ($\tilde{\nu}_\tau$ and $\tilde{\nu}_t$ from $\approx 1.5 - 1.7 \times 10^4$ cm^{-1}) are discussed in the following. The monomer **1** displays two distinct cross peaks at $(\tilde{\nu}_\tau, \tilde{\nu}_t) = (1.58, 1.68) \times 10^4$ cm^{-1} and $(\tilde{\nu}_\tau, \tilde{\nu}_t) = (1.68, 1.58) \times 10^4$ cm^{-1}, which correspond to the absorption maximum at 633 nm and the absorption band of the vibrational progression (as coupling to other chromophores can be excluded) at 595 nm, respectively. Thus, if one of the absorption bands is excited, both bands display a GSB due to the coupling via a common ground state. The diagonal peak at $(\tilde{\nu}_\tau, \tilde{\nu}_t) = (1.68, 1.68) \times 10^4$ cm^{-1} displays only a small GSB signal which indicates either a fast relaxation to lower energetic states, a weaker signal due to a smaller extinction coefficient of the higher energetic band (see Fig. 1), or alternatively an overlapping ESA contribution.

Similar to **1**, **2p** exhibits distinct cross peaks for all T up to 20 ps between its absorption bands at $(\tilde{\nu}_\tau, \tilde{\nu}_t) = (1.55, 1.66) \times 10^4$ cm^{-1} and $(\tilde{\nu}_\tau, \tilde{\nu}_t) = (1.66, 1.55) \times 10^4$ cm^{-1} (645 and 602 nm). Furthermore, a weak higher-energetic diagonal peak at $(\tilde{\nu}_\tau, \tilde{\nu}_t) = (1.66, 1.66) \times 10^4$ cm^{-1} is observable. The increase in lifetime of **2p** compared to **1** can be inferred indirectly by the stronger remaining 2D signal contributions at $T = 70$ ps.

2D spectra of **2m** display a more complex structure than those of **1** and **2p**. Additionally to the cross peaks between the absorption maxima (626 and 598 nm) at $(\tilde{\nu}_\tau, \tilde{\nu}_t) = (1.60, 1.69) \times 10^4$ cm^{-1}, the cross peak $(\tilde{\nu}_\tau, \tilde{\nu}_t) = (1.69, 1.60) \times 10^4$ cm^{-1} is only indicated as the signal at $\tilde{\nu}_t = 1.60 \times 10^4$ cm^{-1} is elongated to larger $\tilde{\nu}_\tau$. Furthermore, a distinct signal at $\tilde{\nu}_t = 1.54 \times 10^4$ cm^{-1} is observable up to 1.3 ps, which displays the coupling from GSB to SE. With evolving population time, the SE decays stronger than the GSB and ESA, leading to a rather small SE signal contribution with remaining GSB and ESA at 70 ps.

For **3**, the three absorption bands at 652, 623, and 598 nm are already visible in the 2D spectrum at $T = 30$ fs as diagonal peaks at $\tilde{\nu}_\tau = \tilde{\nu}_t = 1.53$, 1.61, and 1.67×10^4 cm^{-1}, respectively. Furthermore, the coupling between the latter absorption bands is visible as cross peaks to energetically lower absorption bands below the diagonal ($\tilde{\nu}_t < \tilde{\nu}_\tau$). Already at $T = 300$ fs most of the signal relaxed to a strong combined GSB and SE signal at $\tilde{\nu}_t = 1.53 \times 10^4$ cm^{-1}. For larger T, the SE decays similar to **1**, **2p**, and **2m**, leading to a weak SE with GSB and ESA remaining at 70 ps.

In general, 2D spectroscopy of all studied dyes displays the coupling between the different absorption bands observed in linear absorption. Due to the pulse duration of $\tau_p \approx$ 20 fs and the limited spectral width of the pulses an unambiguous determination of the coupling mechanism (purely excitonic, vibronic, or a mixture of both) of the absorption bands is difficult. This lack in spectral resolution might lead to unambiguous interpretation of cross peak dynamics since signals of different origin (GSB, ESA, SE) with different time evolution can overlap. Extremely broadband laser pulses might lead to a clear discrimination of the origin of the absorption spectra in future studies. Nevertheless, already the current 2D spectra allow us to conclude that there is no significant mixture of isomers in solution. Furthermore, no indication for a photoinduced isomerization process is observed, in contrast to previous studies performed on other merocyanine systems.[15,17–19,21–23] This finding corroborates the excitation energy-dependent TA data presented in Fig. 6, where also no indications of an initial mixture of isomers could be found.

3 Discussion

3.1 Relaxation Model

Having described the results of TA and 2D spectroscopy, we now aim at proposing a general relaxation model for all investigated (multi)chromophoric dyes. Figure 8 shows the relaxation scheme based on the spectroscopic observations for **1**, which indeed can be adapted successfully to all multichromophore dyes (**2p**, **2m**, and **3**) as shown below. Directly upon laser excitation (orange arrow) the population in the first excited state (S_1) moves away

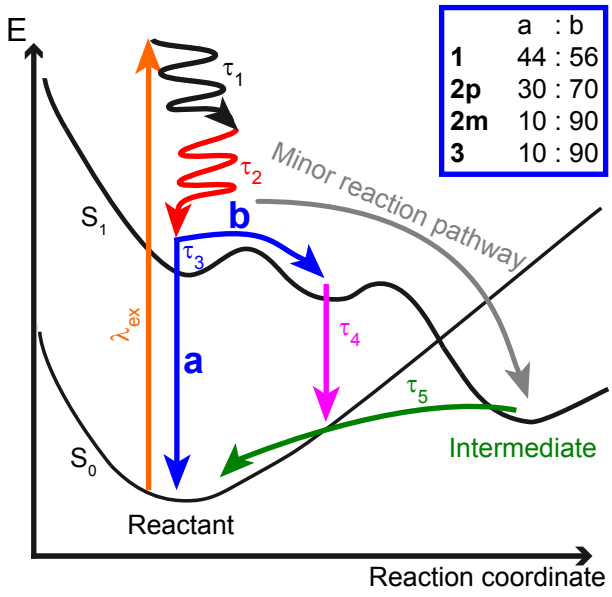

Fig. 8 Relaxation scheme for all studied dyes based on the performed spectroscopic measurements. Upon vertical $S_0 \rightarrow S_1$ excitation (orange, λ_{ex}) the energy relaxes via a wave-packet motion (wiggly arrows) dynamically to a local minimum on the PES which is described by two initial relaxation processes τ_1 (black) and τ_2 (red). From this local minimum the relaxation pathway splits up within τ_3 (blue). Either the system relaxes back to the initial ground state via pathway a, or it further relaxes to another minimum via pathway b. From the latter minimum the relaxation back to the ground state occurs with τ_4 (pink), which determines the S_1 lifetime of the dye. Small spectral indications, i.e., the remaining GSB and photoinduced absorption, suggest a further minor relaxation pathway (gray) to a long-lived intermediate state that relaxes back to the electronic ground state with τ_5 (green), beyond our accessible experimental time window. Results of the target analysis displaying the relaxation pathways ratios for pathway a and b are stated in the inset.

from the Franck–Condon window within $\approx$ 175 fs, which is reflected in τ_1 (black arrow). Furthermore, vibrational relaxation takes place within $\approx$ 1 ps (τ_2, red arrow). The first 2 ps of the relaxation processes are accompanied by ultrafast oscillations with a period of $\approx$ 200 fs, which can be assigned to torsional and vibrational modes of **1**, as previously observed for other merocyanines.[18–20] Therefore, after excitation the system effectively dissipates excess energy by nuclear motions, namely torsion and vibration. It should be mentioned that an assignment of two primary relaxation time scales might be a physically incorrect description as a typical wave-packet motion is a dynamic and not a kinetic process.[31,36,37] However, the description with two kinetic time constants is sufficient to model the data phenomenologically. After these initial relaxation steps, the system is still in the excited state, as observable from the SE and ESA features for all studied molecules. From this stationary point of the PES the proposed relaxation scheme splits up within τ_3 into pathways a and b (labeled blue arrows). Pathway a directly repopulates the electronic ground state S_0, leading to a partial GSB recovery. Most of the population relaxes via pathway b to another minimum of the excited-state PES which is characterized by a shallow SE and a new ESA band at shorter wavelengths. The rise of an ESA band is

explicitly observable as a negative contribution in the blue DADS between 400 and 500 nm for **2p**, **2m**, and **3** (Fig. 5 and Fig. 6). We assign this state to a minimum on the S_1, which relaxes with τ_4 (pink arrow), as it clearly displays ESA and SE features, in contrast to a supposed hot ground state or a relaxed isomer. Thus, the relaxation time scale τ_4 determines the lifetime of the excited state for all dyes. There is probably a further pathway (gray arrow) which leads to a long-lived intermediate and thus to the remaining GSB and photoinduced absorption that may return to the initial ground state only after times of $\tau_5 > 10$ ns (green arrow), compare the DADS in Fig. 3. As the spectral indications of this component are rather small (< 1 mOD), we assign the latter process to a minor relaxation pathway, perhaps evolving through a conical intersection.[25–29,38]

To validate and quantify the proposed relaxation scheme in Fig. 8, a target analysis was performed, investigating the branching ratio from the excited state relaxing with τ_3 towards the ground state (pathway a) and towards the additional minimum in the excited-state PES relaxing with τ_4 (pathway b), respectively. As a feedback for the target fit we required that the GSB from the species-associated difference spectra (SADS, cf. Fig. 9) which relaxes with τ_4 ($SADS_4$, pink) should not have a larger amplitude than $SADS_3$ (blue). For **2p** and **3** such a behavior of the GSB was observed in some spectral regions, as the overlapping ESA contributions decay faster. Therefore, we fitted a branching ratio that could reproduce the GSB at ≈ 650 nm. The ratio b:a (cf. Fig. 8) can be interpreted as an upper limit for the fraction of the excited-state population which relaxes via the longer-lived second minimum on the excited-state minimum, i.e., species $SADS_4$, compared to the fraction of the excited-state population which directly undergoes internal conversion to the ground state. The small remaining signal of $SADS_5$ (green) was reproduced by an additional branching from $SADS_4$ with a ratio of $\ll 1\%$ towards the long-lived species of $SADS_5$ (fixed with 10 ns). For all investigated dyes this scheme could be applied, leading to the ratios summarized in the inset of Fig. 8. For **1** the target model leads to a relaxation branching ratio of almost equal amounts in pathways a and b. This result might be affected by the similarity of the relaxation time scales τ_3 and τ_4 for **1**. Thus, the contributions of the relaxation occurring with τ_3 and τ_4 cannot be distinguished unambiguously. For **2p** a major fraction of the population relaxes by pathway b to $SADS_4$, instead of directly relaxing to the ground state. For **2m** and **3** almost all of the population relaxes via pathway b. The branching ratios of the dyes echo the trend observed for the lifetimes nicely, as for the increase of the lifetime from **1**, over **2p**, to **2m**, and finally to **3**, the branching ratios display a favored relaxation by pathway b.

Similar relaxation models with double-minimum excited-state PES were proposed for other D–A systems, rationalized by a change of electron density or conformation.[20,25–27,30,39–43] Changes of the electron density occur upon localized excitation, i.e., exciting only the D or A moiety of a merocyanine (first minimum), which is equilibrated with a CT state (second minimum).[40–43] Hence, the relaxation might occur from the locally excited or the CT state. For merocyanines which are close to the cyaninelimit, this scenario is rather unlikely as the delocalization

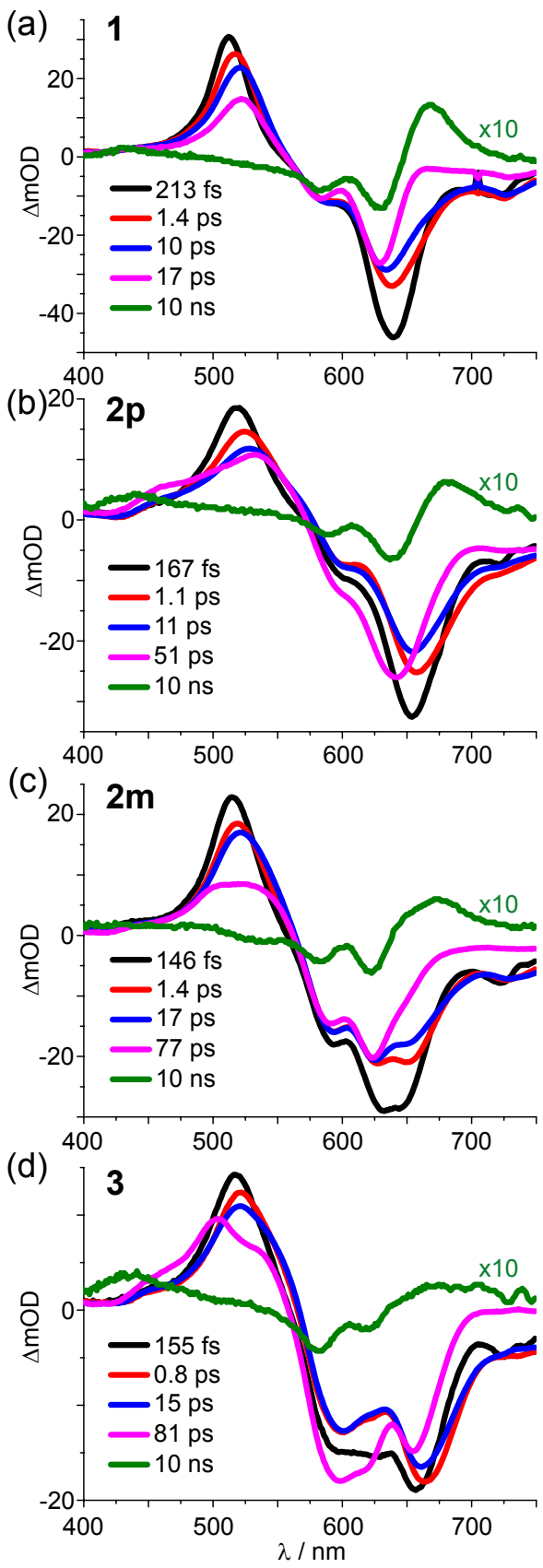

Fig. 9 SADS of **1** (a), **2p** (b), **2m** (c), and **3** (d) for transient absorption data with excitation pulses centered at 630 nm (see gray spectrum in Fig. 1b).

of the electron density does not change upon excitation.[13] Still, it cannot be excluded that an initially excited CT state relaxes to an additional CT state which displays a complete charge separation. Additionally to changes in the electron density, the double minimum on the excited-state PES was proposed to originate from conformational changes, e.g., a planarized or twisted structure. Such structural changes break the conjugation of the π-electron system and might lead to an isomerization as observed for similar merocyanine systems.[15–20] The oscillatory behavior within the first few picoseconds of the relaxation for **1** indicates enhanced vibrational and rotational motion of the polyene linker upon excitation. Additionally, the small photoinduced absorption feature up to $T = 3.6$ ns indicates an isomerization via the minor relaxation pathway. Thus, the double minimum on the excited-state PES might be based on structural changes in the excited state, which is followed by a structural relaxation back to the initially excited conformation.

3.2 Chromophore Interactions

From the described relaxation model and observed trends, information about the chromophore interaction mechanism can be inferred. For classical Förster energy transfer, fluorescence of a chromophore is required.[2] As almost no fluorescence of the chromophores was observed, this mechanism cannot be applied to describe the system under investigation. Another mechanism for energy transfer is described by Dexter.[3] It requires that the chromophores are in close distance to each other, such that the chromophore wavefunctions overlap. Due to the separation of the chromophores via the benzene linker (≈ 0.5 nm), we assume this mechanism to be rather unlikely. However, due to the electron delocalization over the polymethine bridge it still might be possible to describe the energy transfer with this theory. Dexter-energy transfer would lead to a charge-transfer state by electron transfer, which can be observed by TA experiments. For **2m** a longer excited-state lifetime compared to **2p** can be observed while the distance is smaller in **2m**. Thus, Dexter-energy transfer seems also not applicable. The presence of donor and acceptor subunits in merocyanines allows an intramolecular charge-transfer (ICT) state on a single merocyanine.[4,6] Such an ICT state can be modelled as a second local minimum of the excited-state PES as observed for **1** (cf. Fig. 8). As one can see from the target analysis in **1** the ratio between the two relaxation pathways is rather similar, while it increases towards pathway b with increasing number of chromophores. Hence, via electrostatic interactions between these highly dipolar ($\mu_g = 13.1$ D) chromophores in the multichromophoric systems (**2p**, **2m**, and **3**) the barrier between the two S_1 minima is varied due to a stabilization of the ICT state. This leads to an increase of the excited-state lifetime for the multichromophoric merocyanines. Similar results were observed by Burda *et al.* for the protonation of a merocyanine dye,[30] and by Kahan and Wand *et al.*, who observed a stabilization of the ICT state by the polarity of the solvent.[31] In detail, the para-oriented compound (**2p**) stabilizes the ICT state less than the meta (**2m**) compound. The stabilization is reflected in the excited-state lifetimes: while the para-substituted dimer **2p** already displayed an excited-state lifetime three times longer compared to **1**, the lifetime of the meta-linked bis-merocyanine dye **2m** was increased by even a factor of ≈ 4.5. However, including a third chromophore in meta position (**3**) does not influence the ICT state significantly. Thus, the third chromophore is more a spectator whilst the second contributes to the stabilization of the ICT state of the excited first.

4 Conclusion

Merocyanines provide versatile options of structural variation to tune their molecular properties. Exemplarily, merocyanines can be varied by changing the donor and acceptor moiety, the length of the connecting polymethine chain, and the environment (solvent). Another tuning parameter, often used when creating large molecular systems, e.g., aggregates, is the chromophore–chromophore interaction.

In our study the influence of chromophore–chromophore interactions on the electronic properties of merocyanines was investigated via a systematic molecular series of merocyanine dyes. In the molecular series the position and number of merocyanines directly linked to a benzene unit was varied and compared to a single merocyanine attached to the benzene bridge.

Linear absorption displayed obvious changes between the mono-merocyanine and the bis- and tris-merocyanine dyes, respectively. Transient absorption and 2D spectroscopy data led to a relaxation model which described all measurements. The relaxation model comprises two local minima in the first excited state. Directly after laser excitation a coherent wave packet could be observed, which relaxes into the first local minimum. From there the relaxation splits up either directly towards the ground state as internal conversion or towards another local minimum. This second local minimum on the potential energy surface is assigned to an intramolecular charge-transfer (ICT) state. Due to the varying substitution pattern with dipolar chromophores in the neighborhood the ICT state is stabilized in different amounts, leading to a strong variation in excited-state lifetime.

This study investigated fundamental changes of the relaxation dynamics for dipolar merocyanines upon introducing interactions to other dipolar merocyanine units in close vicinity. Unlike other approaches, e.g., based on intermolecular interactions or tuning the lifetime by changing the environment, the presented results offer the tunability via variation of the substitution pattern. Since this approach can also be applied to other molecular systems, the observations provide valuable information for tuning the excited-state lifetime of similar dipolar donor–acceptor dyes.

5 Materials and Methods

All samples were prepared in dichloromethane (DCM) such that they show an absorbance of ≈ 0.3 OD at the respective excitation wavelength in a flow cell with 200 μm sample thickness. Steady-state absorption spectra were measured with a Jasco V-670 UV-Vis spectrometer. All ultrafast spectroscopy experiments were performed in a transient-absorption setup which was described in Ref. 16 in detail. Briefly, a Ti:Sa oscillator and a regenerative amplifier (Solstice, Spectra Physics) provided 100 fs pulses with a central wavelength of 800 nm at a repetition rate

of 1 kHz. A part of the output was used to pump a noncollinear optical parametric amplifier (Topas White, Light Conversion) to generate the excitation pulses. These pulses were compressed to about 20 fs via a home-built pulse shaper consisting of a two-layer liquid-crystal phase mask (SLM-640, CRI) in $4f$ configuration. Pulse characterization was performed via pulse-shaper-assisted collinear frequency-resolved optical gating (cFROG).[44,45] A small fraction of the 800 nm pulses was used to pump a linearly moving CaF_2 plate, which created a white-light continuum covering the whole visible spectral region. The pump–probe delay T was set up to ≈ 3.6 ns by delaying the probe beam with a mechanical translation stage. Every second pump pulse was blocked by a chopper driven at 500 Hz. This signal was detected shot-to-shot using a spectrometer (Acton SP2500i, Princeton Instruments) with an attached CCD camera. Magic angle configuration was used to eliminate effects of anisotropy in TA and 2D spectroscopy measurements.[46] TA data evaluation was performed via global analysis[47] with the software package Glotaran[48] based on the R-package TIMP[49]. In addition, a target analysis was performed with the same software. The fitting routine accounted for the instrument response function, the chirp of the white-light continuum, and the coherent artifact.[50–52] Coherent 2D spectroscopy was performed in the previously mentioned TA setup with laser excitation pulses depicted in Fig. 1 (gray). To obtain 2D data in TA geometry, the coherence time τ was varied by the pulse shaper, from 0 fs up to 109.5 fs in 1.5 fs steps, for every T, applying a three-fold phase-cycling scheme.[53–55] Purely absorptive 2D spectra were generated by Fourier transformation along τ and taking the real part. 2D spectra for short population times were chirp corrected by measuring T from -600 to $+600$ fs in steps of 30 fs and subsequently from $T = 700$ fs to $T = 1.3$ ps in 100 fs steps.[56] 2D spectra for population times from 10 to 70 ps were not chirp corrected.

Acknowledgments

We thank the Free State of Bavaria for financial support through the "Solar Technologies Go Hybrid (Soltech)" program and the German Research Foundation (DFG) for funding within the Research Unit "Light-Induced Dynamics in Molecular Aggregates" (FOR 1809) as well as within the Graduate College "Control of Electronic Properties of Assemblies of pi-Conjugated Molecules" (GRK 1221). AS thanks the German National Academic Foundation (Studienstiftung des deutschen Volkes) for a scholarship.

References

1 M. Kasha, H. R. Rawls and M. Ashraf El-Bayoumi, *Pure Appl. Chem.*, 1965, **11**, 371–392.
2 T. Förster, *Naturwissenschaften*, 1946, **33**, 166–175.
3 D. L. Dexter, *J. Chem. Phys.*, 1953, **21**, 836–850.
4 P. Pasman, F. Rob and J. W. Verhoeven, *J. Am. Chem. Soc.*, 1982, **104**, 5127–5133.
5 M. Klessinger, *Chemie in unserer Zeit*, 1978, **12**, 1–11.
6 A. V. Kulinich and A. A. Ishchenko, *Russ. Chem. Rev.*, 2009, **78**, 141–164.
7 F. Würthner, R. Wortmann and K. Meerholz, *ChemPhysChem*, 2002, **3**, 17–31.
8 B. Kippelen, F. Meyers, N. Peyghambarian and S. R. Marder, *J. Am. Chem. Soc.*, 1997, **119**, 4559–4560.
9 L. Huang, M. Stolte, H. Bürckstümmer and F. Würthner, *Adv. Mater.*, 2012, **24**, 5750–5754.
10 A. Arjona-Esteban, J. Krumrain, A. Liess, M. Stolte, L. Huang, D. Schmidt, V. Stepanenko, M. Gsänger, D. Hertel, K. Meerholz and F. Würthner, *J. Am. Chem. Soc.*, 2015, **137**, 13524–13534.
11 A. Liess, L. Huang, A. Arjona-Esteban, A. Lv, M. Gsänger, V. Stepanenko, M. Stolte and F. Würthner, *Adv. Funct. Mater.*, 2015, **25**, 44–57.
12 A. Lv, M. Stolte and F. Würthner, *Angew. Chem. Int. Ed.*, 2015, **54**, 10512–10515.
13 F. Würthner, G. Archetti, R. Schmidt and H.-G. Kuball, *Angewandte Chemie*, 2008, **120**, 4605–4608.
14 C. Brückner, C. Walter, M. Stolte, B. Braïda, K. Meerholz, F. Würthner and B. Engels, *J. Phys. Chem. C*, 2015, **119**, 17602–17611.
15 A. Yartsev, J.-L. Alvarez, U. Åberg and V. Sundström, *Chem. Phys. Lett.*, 1995, **243**, 281–289.
16 M. Kullmann, S. Ruetzel, J. Buback, P. Nuernberger and T. Brixner, *J. Am. Chem. Soc.*, 2011, **133**, 13074–13080.
17 Z. Wang, S. Chu, S. Wang and Q. Gong, *J. Chem. Phys.*, 2012, **137**, 164502.
18 S. Ruetzel, M. Diekmann, P. Nuernberger, C. Walter, B. Engels and T. Brixner, *J. Chem. Phys.*, 2014, **140**, 224310.
19 C. Walter, S. Ruetzel, M. Diekmann, P. Nuernberger, T. Brixner and B. Engels, *J. Chem. Phys.*, 2014, **140**, 224311.
20 P. Nuernberger, S. Ruetzel and T. Brixner, *Angew. Chem. Int. Ed.*, 2015, **54**, 11368–11386.
21 R. S. S. Kumar, L. Lüer, D. Polli, M. Garbugli and G. Lanzani, *Opt. Mater. Express*, 2011, **1**, 293.
22 N. P. Ernsting, *Chem. Phys. Lett.*, 1989, **159**, 526–531.
23 N. Tamai and H. Masuhara, *Chem. Phys. Lett.*, 1992, **191**, 189–194.
24 J. Buback, P. Nuernberger, M. Kullmann, F. Langhojer, R. Schmidt, F. Würthner and T. Brixner, *J. Phys. Chem. A*, 2011, **115**, 3924–3935.
25 A. Sanchez-Galvez, P. Hunt, M. A. Robb, M. Olivucci, T. Vreven and H. B. Schlegel, *J. Am. Chem. Soc.*, 2000, **122**, 2911–2924.
26 P. Nuernberger, G. Vogt, G. Gerber, R. Improta and F. Santoro, *J. Chem. Phys.*, 2006, **125**, 044512.
27 G. Vogt, P. Nuernberger, G. Gerber, R. Improta and F. Santoro, *J. Chem. Phys.*, 2006, **125**, 044513.
28 X. F. Xu, A. Kahan, S. Zilberg and Y. Haas, *J. Phys. Chem. A*, 2009, **113**, 9779–9791.
29 A. Toniolo, G. Granucci and T. J. Martínez, *J. Phys. Chem. A*, 2003, **107**, 3822–3830.
30 C. Burda, M. H. Abdel-Kader, S. Link and M. A. El-Sayed, *J. Am. Chem. Soc.*, 2000, **122**, 6720–6726.
31 A. Kahan, A. Wand, S. Ruhman, S. Zilberg and Y. Haas, *J. Phys. Chem. A*, 2011, **115**, 10854–10861.

32 F. Koch, M. Stolte, D. Bialas, A. Zitzler-Kunkel, A. Steinbacher, T. Brixner and F. Würthner, *in preparation*, 2016.

33 J. A. Cina, P. A. Kovac, C. C. Jumper, J. C. Dean and G. D. Scholes, *J. Chem. Phys.*, 2016, **144**, 175102.

34 M. H. Vos, F. Rappaport, J.-C. Lambry, J. Breton and J.-L. Martin, *Nature*, 1993, **363**, 320–325.

35 Q. Wang, R. W. Schoenlein, L. A. Peteanu, R. A. Mathies and C. V. Shank, *Science*, 1994, **266**, 422–424.

36 A. Douhal, F. Lahmani and A. H. Zewail, *Chem. Phys.*, 1996, **207**, 477–498.

37 C. Schriever, S. Lochbrunner, A. R. Ofial and E. Riedle, *Chem. Phys. Lett.*, 2011, **503**, 61–65.

38 E. Teller, *J. Phys. Chem.*, 1937, **41**, 109–116.

39 I. H. M. van Stokkum, T. Scherer, A. M. Brouwer and J. W. Verhoeven, *J. Phys. Chem.*, 1994, **98**, 852–866.

40 K. A. Zachariasse, M. Grobys, T. von der Haar, A. Hebecker, Y. V. Il'ichev, Y. B. Jiang, O. Morawski and W. Kühnle, *J. Photochem. Photobiol. A: Chem.*, 1996, **102**, 59–70.

41 Z. R. Grabowski, K. Rotkiewicz and W. Rettig, *Chem. Rev.*, 2003, **103**, 3899–4032.

42 T. Yoshihara, S. I. Druzhinin and K. A. Zachariasse, *J. Am. Chem. Soc.*, 2004, **126**, 8535–8539.

43 S. I. Druzhinin, N. P. Ernsting, S. A. Kovalenko, L. P. Lustres, T. A. Senyushkina and K. A. Zachariasse, *J. Phys. Chem. A*, 2006, **110**, 2955–2969.

44 I. Amat-Roldán, I. Cormack, P. Loza-Alvarez, E. Gualda and D. Artigas, *Opt. Express*, 2004, **12**, 1169–1178.

45 A. Galler and T. Feurer, *Appl. Phys. B*, 2008, **90**, 427–430.

46 S. Schott, A. Steinbacher, J. Buback, P. Nuernberger and T. Brixner, *J. Phys. B: At. Mol. Opt. Phys.*, 2014, **47**, 124014.

47 I. H. M. van Stokkum, D. S. Larsen and R. van Grondelle, *Biochimica et Biophysica Acta (BBA) - Bioenergetics*, 2004, **1657**, 82–104.

48 J. J. Snellenburg, S. P. Laptenok, R. Seger, K. M. Mullen and I. H. M. van Stokkum, *J. Stat. Softw.*, 2012, **49**, 1–22.

49 K. M. Mullen and I. H. M. van Stokkum, *J. Stat. Softw.*, 2007, **18**, 1–46.

50 K. Ekvall, P. van der Meulen, C. Dhollande, L.-E. Berg, S. Pommeret, R. Naskrecki and J.-C. Mialocq, *J. Appl. Phys.*, 2000, **87**, 2340.

51 M. Rasmusson, A. N. Tarnovsky, E. Åkesson and V. Sundström, *Chem. Phys. Lett.*, 2001, **335**, 201–208.

52 B. Dietzek, T. Pascher, V. Sundström and A. Yartsev, *Laser Phys. Lett.*, 2007, **4**, 38–43.

53 H.-S. Tan, *J. Chem. Phys.*, 2008, **129**, 124501.

54 Z. Zhang, K. L. Wells, E. W. J. Hyland and H.-S. Tan, *Chem. Phys. Lett.*, 2012, **550**, 156–161.

55 J. A. Myers, K. L. Lewis, P. F. Tekavec and J. P. Ogilvie, *Opt. Express*, 2008, **16**, 17420–17428.

56 P. A. Tekavec, K. L. Lewis, F. D. Fuller, J. A. Myers and J. P. Ogilvie, *IEEE J. Sel. Top. Quantum Electron.*, 2012, **18**, 210–217.